Advance Testing and Modeling of Dredged Sediments for Beneficial Use

FINAL REPORT April 2025

Submitted by:

Tyler J. Oathes, Ph.D. Assistant Professor

Robert Miskewitz, Ph.D. Professor

Mahdi Talebi Graduate Student Researcher

Rutgers University
Department of Civil and Environmental Engineering
500 Bartholomew Road
Piscataway, NJ, -8854

Scott Douglas
New Jersey Department of Transportation

In cooperation with

Rutgers, The State University of New Jersey
And
New Jersey Department of Transportation
And
U.S. Department of Transportation
Federal Highway Administration

Disclaimer Statement

The contents of this report reflect the views of the authors, who are responsible for the facts and the accuracy of the information presented herein. This document is disseminated under the sponsorship of the Department of Transportation, University Transportation Centers Program, in the interest of information exchange. The U.S. Government assumes no liability for the contents or use thereof.

The Center for Advanced Infrastructure and Transportation (CAIT) is a Regional UTC Consortium led by Rutgers, The State University. Members of the consortium are Atlantic Cape Community College, Columbia University, Cornell University, New Jersey Institute of Technology, Polytechnic University of Puerto Rico, Princeton University, Rowan University, SUNY - Farmingdale State College, and SUNY - University at Buffalo. The Center is funded by the U.S. Department of Transportation.

1. Report No. CAIT-UTC-REG76	2. Government Accession No.).		
4. Title and Subtitle		5. Report Date			
Advanced Testing and Modeli	April 2025				
for Beneficial Use	6. Performing Organizati CAIT/Rutgers, The Stat New Jersey				
TECHNICAL 7. Author(s) Tyler J. Oathes (https://orcid.org, Robert Miskewitz (https://orcid.c	8. Performing Organizati CAIT-UTC-REC				
9. Performing Organization Name and Address Center for Advanced Infrastructure	•	10. Work Unit No.			
Rutgers, The State University of Ne		11. Contract or Grant No).		
100 Brett Road Piscataway, NJ 088	54	69A3551847102			
12. Sponsoring Agency Name and Address		13. Type of Report and P	eriod Covered		
Center for Advanced Infrastructure	and Transportation	Final Report			
Rutgers, The State University of Ne	•	1/1/2023 - 4/15/2025			
100 Brett Road Piscataway, NJ 0883	14. Sponsoring Agency (Code			
15. Supplementary Notes U.S. Department of Transportation/OST-R 1200 New Jersey Avenue, SE Washington, DC 20590-0001					
This study investigates the shear te harbor under direct simple shear lowere stabilized with Portland ceme confining pressures and curing dura stress paths. Additionally, unconfin baseline for comparing the DSS restesting, the experimental results wand PM4Silt (Ziotopoulou and Boulaccurately simulating the deformat of structures constructed with stab avenues for incorporating stabilized however, further work is required to	ading conditions experimentally int and subjected to direct simple ations to elucidate the impact on ed compressive strength (UCS) to ults with methods commonly use ere used to calibrate numerical manger 2019) constitutive models ion tendencies and providing me ilized sediments. The findings of disediments into projects with method utilize these results in practice.	and numerically. For shear loading with the stress-strain reserved in practice. Follow nodels using the Moto evaluate the post thods for system leading research may core rigorous designate.	our sediments on varying esponses and od to provide a wing the lab ohr-Coulomb tential of evel modeling open new		
17. Key Words stabilized sediment, ground ir	18. Distribution Stat	ement			
beneficial use	nprovement,				
Deficilitial use					
19. Security Classification (of this report)	20. Security Classification (of this page)	21. No. of Pages	22. Price		

Unclassified

Total 27

Unclassified

Acknowledgments

The research team would like to acknowledge the Rutgers Center for Advanced Infrastructure and Transportation and the United States Department of Transportation University Transportation Research Center program for their support of this work. Additionally, the authors appreciate the assistance of graduate research assistant Kaleb Arnold and undergraduate research assistants Jonathan Ho and Eva Pharande for their help with different portions of the experimental testing.

Table of Contents

1.	Background1
2.	Methodology1
2	1 Field Sampling2
2	2 Characterization3
2	3 Strength Testing4
2	4 Laboratory Sample Preparation5
2	5 Modeling Considerations5
3.	Experimental Strength Testing Results5
3	1 DSS5
3	2 UCS12
4.	Numerical Modeling13
4	1 Mohr-Coulomb with experimentally interpreted properties14
4	2 Mohr-Coulomb with adjusted properties15
4	3 PM4Silt Modeling17
5.	Conclusions
6.	References
	of Figures
_	re 1: Approximate sediment sampling locations (Google Earth)
_	re 2: Sampled sediments (a) Atterberg limits and (b) particle size distributions4
_	re 3:(a) Peak shear stress and (b) peak shear stress ratio versus vertical confining pressure6
_	re 4: Monotonic stress-strain responses for the sediments stabilized with 4% cement after and 14 days of curing
_	re 5: Monotonic stress-strain responses expressed as stress-ratios for the sediments ilized with 4% cement after 3, 7, and 14 days of curing
	re 6: Monotonic stress-paths for the sediments stabilized with 4% cement after 3, 7, and 14 of curing8
_	re 7: Monotonic stress paths expressed as stress ratios for the sediments stabilized with cement after 3, 7, and 14 days of curing9
_	re 8: Stress-strain responses and stress paths for Newtown Creek with 4% and 8% added ent after 3, 7, and 14 days of curing10
_	re 9: Impact of long-term curing on stress-strain response of Newark Bay sediment tested σ'_{vc} = 100 kPa11

Figure 10: Unconfined compressive strength versus (a) density, (b) moisture content, and (c) curing length12
Figure 11: Measured peak shear stress ratio versus the maximum shear stress ratio modeled using (a) interpreted and (b) optimized friction angle and cohesion14
Figure 12: Comparison between the measured and predicted response using the interpreted properties expressed as (a,c,e) stress strain responses and (b,d,e) stress paths for Newark Bay after 3 days curing (a,b), Newark Bay after 7 days curing (c,d), and Wallabout Channel after 14 days of curing (e,f)
Figure 13: Experimentally interpreted versus measured (a) friction angle and (b) cohesion 16
Figure 14: Comparison between the measured and predicted response using the adjusted properties expressed as (a,c,e) stress strain responses and (b,d,e) stress paths for Newark Bay after 3 days curing (a,b), Newark Bay after 7 days curing (c,d), and Wallabout Channel after 14 days of curing (e,f)
Figure 15: Comparison between the measured and predicted response using PM4Silt expressed as (a,c,e) stress strain responses and (b,d,e) stress paths for Newark Bay after 3 days curing (a,b), Newark Bay after 7 days curing (c,d), and Wallabout Chanel after 14 days of curing
List of Tables Table 1: Sediments sampled and approximate locations
Table 2: Summary of relevant sediment properties4
Table 3: Interpreted and optimized friction angle and cohesion11
Table 4: Results of UCS testing program13
Table 5: Parameters for PM4Silt calibrations

1. BACKGROUND

Dredging operations are regularly performed to maintain required depths in navigation channels and port access worldwide, including regularly in the New Jersey and New York harbor. As a result, several millions cubic yards of sediment are transferred from aquatic to terrestrial environments annually (Lirer et al., 2017; Snellings et al., 2016). These sediments often contain contamination, have high water contents and poor geotechnical properties, notably low strength and stiffness. Several management strategies are available for handling these sediments; however, treating them with pozzolanic additives, such as Portland cement, is one of the most common and cost-effective approaches. This has a two-fold impact: (1) it enhances their geotechnical properties through stabilization and (2) it freezes the contaminants in the sediment matrix through solidification. Although utilizing stabilizers results in improved materials, the beneficial use of improved sediments is typically confined to low-risk and non-structural applications, such as road bases, landfill covers, golf courses, and parking lots. Allowing more use cases, including structural applications, is essential to create additional avenues for increased utilization. This requires a thorough understanding of the strength and deformation characteristics of stabilized sediment.

Numerous research and testing programs have utilized unconfined compressive strength (UCS) tests to investigate the effectiveness of sediment stabilization on a wide range of sediments using different combinations of admixtures, dosages, curing periods, and curing conditions (e.g., Chew et al. 2004; Horpibulsuk et al. 2010, 2011; Pakbaz and Alipour 2012; Liu and Ryan 2013; Voottipruex and Jamsawang 2014; Ranaivomanana et al. 2018; Chompoorat et al. 2019). These testing programs have generally shown that different stabilization methods can be developed to obtain the required specifications for a given nonstructural beneficial use project as these typically only rely on achieving a minimum strength threshold rather than specific stress-deformation performance. However, UCS test limitations are well known, including the unknown stress conditions during loading and how stress-strain responses do not accurately replicate field behavior due to the lack of confinement and consolidation during shearing. Therefore, while UCS tests are likely adequate for non-structural applications, they are not sufficient to evaluate or design more structural beneficial uses with stabilized sediments. To use these sediments as structural fill (e.g., bulkhead fill, roadway subbase, embankment construction), assessing and modeling the stress-deformation behavior becomes important.

To utilize sediment in more advanced beneficial uses, more advanced testing techniques such as triaxial compression or direct simple shear (DSS) need to be considered. These techniques provide a deeper understanding of a soil/sediments engineering performance (both strength and deformation) under loading conditions that better mimic the field (e.g., overburden pressure and/or consolidation). Only a few experimental programs have utilized these techniques on stabilized sediments (e.g., Dermatas et al. 2003, Suzuki et al. 2014, Sariosseiri and Muhunthan 2009, Horpibulsuk et al. 2004, Grubb et al. 2010, Maher et al. 2013). However, these experimental programs primarily focus on evaluating the friction angle and cohesion with limited to no information available on the deformation tendencies. Although Talebi et al. (2025) demonstrated that the cemented sediment tested under DSS loading did not undergo brittle failure and experienced little to no post peak strength loss, it is unclear whether this result can be generalized to other materials and stabilized sediments since the experimental programs previously made only limited discussion the material's deformation tendencies. Additional research is required to

methodically assess the shear tendencies of different stabilized sediments to assess whether dredged sediment is appropriate for structural beneficial uses.

This study investigates the shear tendencies of soft sediments from the New York and New Jersey harbor under direct simple shear loading conditions experimentally and numerically. Four sediments were stabilized with Portland cement and subjected to direct simple shear loading with varying confining pressures and curing durations to elucidate the impact on the stress-strain responses and stress paths. Additionally, unconfined compressive strength (UCS) tests were performed to provide a baseline for comparing the DSS results with methods commonly used in practice. Following the lab testing, the experimental results were used to calibrate numerical models using the Mohr-Coulomb and PM4Silt (Ziotopoulou and Boulanger 2019) constitutive models to evaluate the potential of accurately simulating the deformation tendencies and providing methods for system level modeling of structures constructed with stabilized sediments. The findings of this research may open new avenues for incorporating stabilized sediments into projects with more rigorous design criteria; however, further work is required to utilize these results in practice.

2. METHODOLOGY

This work investigated the engineering performance (both strength and deformation) of stabilized, fine-grained New York and New Jersey Harbor sediments under loading conditions that better mimic the loading conditions encountered in practice. The experimental results were then used to calibrate different constitutive models of varying complexities. Following is a brief description of the approaches used.

2.1 FIELD SAMPLING

Samples were collected from four locations around the New York and New Jersey Harbor. Sampled locations are indicated by yellow pins in Fig. 1 below and summarized in Table 1; sampling locations were selected to produce a range of different sediment types with varying levels of industrial contamination and organic contents. Surficial sediments were sampled using a ponar grab sampler to extract sediments to a depth of approximately 9" to 12". Between 9 and 15.6 kg of sediment were sampled at each location. Prior to testing and characterization, sediments were screened using a #4 sieve (4.75 mm particle size) to remove larger shell fragments, debris, and particles which might impact subsequent strength testing; a minimal amount of material was removed during screening.



Figure 1: Approximate sediment sampling locations (Google Earth)

Table 1: Sediments sampled and approximate locations

Sediment	Symbol	Approximate Latitude	Approximate Longitude	Approximate Sampled Mass (kg)
Newark Bay	NB	74.167°W	40.649°N	15.6
Newtown Creek	NC	73.932°W	40.715°N	13.4
Wallabout Channel	WC	73.968°W	40.704°N	15.6
Bayway Creek	BC	74.203°W	40.634°N	9.0

2.2 CHARACTERIZATION

Sediments were characterized following the relevant ASTM standards. Fig. 2a and 2b present the Atterberg limits and particle size distributions, respectively, while Table 2 summarizes the sediment properties. All sediments were fine-grained with high natural moisture contents (> 135%) and organic contents (> 7.5%). The specific gravities of the sediments range from 2.27 for NC to 2.62 for WC, with higher specific gravities generally correlated with lower organic contents, as expected. The respective particle size distributions (Fig. 2b) slightly differ which may influence the behavior of the sediment under shear. NB and NC have sand contents of approximately 13%, whereas WC and BC have sand contents of approximately 5%. Additionally, the fines content (silts and clays) is approximately evenly split between clay and silt particles for all sediments except for the WC sediment which has approximately 9 times more silt than clay. All sediments plot below the A-line in the Atterberg limit plot indicating they behave like high plasticity silts or organic silts, except for the WC sediment which plots nearly on top of the A-line.

Total PAH (tPAH) concentration was found via extractions obtained using EPA Method 345A and EPA Method 3610B which were analyzed for PAH-38 using gas chromatography-triple quadruple mass spectrometry in multiple reaction monitoring mode. The NB and WC sediments have tPAH values between approximately 10 and 20 mg/kg-ds whereas NC and BC have between tPAH between 300 and 400 mg/kg-ds, a significantly higher value. The two disparate tPAH ranges may influence the observed responses due to the impact of tPAH on the cement interaction with water in the sediment-water matrix.

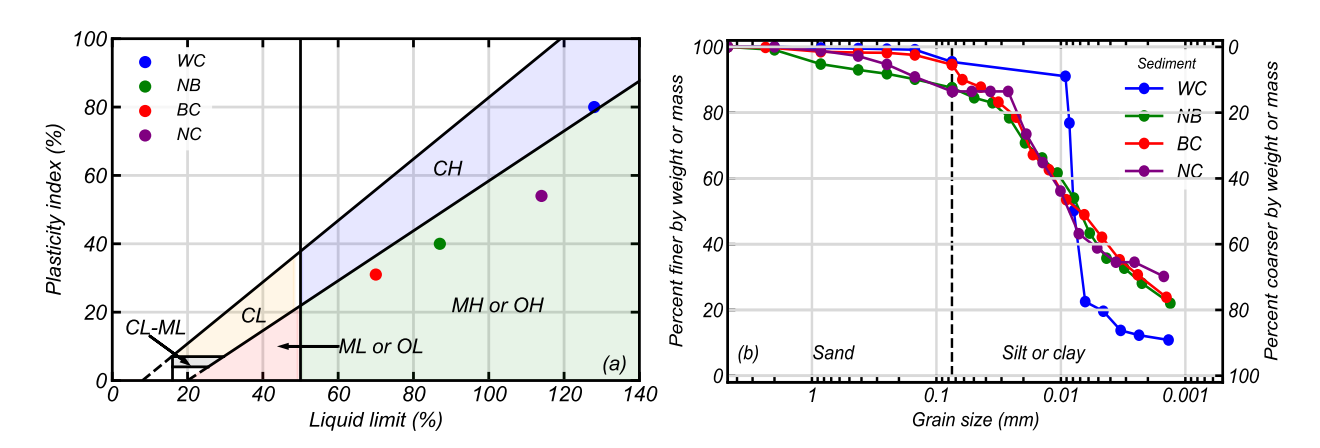


Figure 2: Sampled sediments (a) Atterberg limits and (b) particle size distributions

Table 2: Summary	of relevant se	ediment properties
------------------	----------------	--------------------

Physical index	ASTM Standard	NB	NC	WC	ВС
Water content (%)	D2216	139	245	272	116
Specific gravity	D854	2.57	2.27	2.62	2.4
Liquid Limit (LL) (%)	D4318	87	114	128	70
Plastic Limit (PL) (%)	D4318	40	60	48	38
Plastic Index (PI) (%)	D4318	47	54	80	31
Clay fraction (%)	D7928	43.4	38.9	10.8	49.0
Silt fraction (%)	D6913/7928	44.2	47.6	84.6	45.7
Sand fraction (%)	D6913	12.4	13.5	4.6	5.4
Organic content (%)	D2974	7.6	25.3	12.6	12.4
USCS	D2478	ОН	ОН	ОН	ОН
tPAH (mg/kg-ds)		20.2	308	13.9	377

2.3 STRENGTH TESTING

Sediment performance was assessed using direct simple shear (DSS) testing. DSS tests were performed to 15% shear strain at a strain rate of 1 %/min using a servo controlled VJ Tech DSS device (United Kingdom). Tests were performed under constant volume conditions with initial vertical effective stresses of (σ'_{vc}) of 25, 100, and 400 kPa on 50 mm diameter specimens. Consolidation was performed using a load increment ratio of 2.0 with consolidation step lengths approximately equal to the time to 95% consolidation (T_{95}) and the final step length approximately double T_{95} . The primary test series was performed after 3, 7, and 14 days of curing for all four sediments. Three additional DSS tests were performed with NC sediment with σ'_{vc} = 100 kPa after 28 days, 3 months, and 6 months of curing to evaluate the impact of further curing. Over 45 DSS tests were conducted in total.

Unconfined compression strength (UCS) tests were performed using an ELE TriTest 50 load frame (United Kingdom) with data electronically captured using ELE DS 7.1 software. UCS tests were performed at a strain rate of 1 %/min in triplicate after 3, 7, and 14 days of curing. A total of 45 UCS tests were performed.

2.4 LABORATORY SAMPLE PREPARATION

Prior to sample creation, each sediment was thoroughly homogenized by mixing with an electric drill using a paddle blade attachment at medium speed for several minutes. The baseline test series utilized a mix design of 4% portland cement by wet weight. An additional mix design of 8% portland cement by wet weight was used with the NC sediment to evaluate the impact of cement content. The cement was added as a slurry (100% moisture content) and introduced using a stand mixer with a paddle blade attachment for approximately five minutes at alternating speeds until the cement slurry and sediment was homogenized and fully mixed. After cement addition, the sediment was placed into plastic cylindrical split molds with a diameter of 50 mm and a height of 100 mm for curing. Molds were filled in approximately three equal lifts and were hand tapped to remove entrapped air bubbles. Prepared sediment cores were placed inside a closed cooler at room temperature and cured for 3, 7, and 14 days. Samples were produced in quadruplet for each designated curing length. Three samples were used for UCS testing and one core was utilized for DSS testing. The DSS core produced three specimens with heights of approximately 21 mm.

2.5 Modeling Considerations

Numerical simulations of the DSS tests were performed using the commercial finite difference program FLAC 8.1 (Itasca 2019) with the Mohr-Coulomb and user-defined PM4Silt (Ziotopoulou and Boulanger 2019) constitutive models. The two models were selected to investigate the ability of constitutive models with different complexity levels capture the strength and deformation tendencies of stabilized sediment. The Mohr-Coulomb model was selected to mimic a relatively simple constitutive model which can be directly incorporated into a range of analysis types including limit equilibrium and empirical correlations, as well as the more advanced finite difference method illustrated herein. PM4Silt was selected to illustrate more advanced constitutive models which have been developed for use in more complex analyses including dynamic loading conditions. Experimental tests were simulated using single element simulations of constant volume DSS loading. Tests were performed at the same overburden pressure as the experimental tests and assumed an at-rest lateral earth pressure coefficient (K_o) of 0.5.

3. EXPERIMENTAL STRENGTH TESTING RESULTS

3.1 DSS

The peak shear stress (τ_{pk}) increases and the peak shear stress ratio (τ_{pk}/σ'_{vc}) decreases with an increasing σ'_{vc} for all sediments. This is consistent with expectations for a stress-dependent material with light cementation. The τ_{pk}/σ'_{vc} increases as σ'_{vc} decreases because the cement content contributes a more significant portion of τ_{pk} at low σ'_{vc} compared with higher σ'_{vc} where the stress-dependent (frictional) component contributes more to the τ_{pk} . Figure 3 below presents τ_{pk} and τ_{pk}/σ'_{vc} versus σ'_{vc} for the DSS tests. In some tests with $\sigma'_{vc} = 25$ kPa, an initial τ_{pk} is mobilized before subsequent strain-hardening begins. For these tests the reported τ_{pk} were measured prior to the subsequent strain-hardening. The standard deviation of τ_{pk} increases as σ'_{vc} increases whereas the standard deviation decreases for τ_{pk}/σ'_{vc} as σ'_{vc} increases. At $\sigma'_{vc} = 25$ kPa, all DSS test mobilize τ_{pk} within an approximate 5 kPa range which results in a τ_{pk}/σ'_{vc} ranging between \sim 0.43 and 0.73. Both the sediment type and curing length has a large influence on both τ_{pk}/σ'_{vc} and τ_{pk} . It appears that the decrease in strength ratio follows an exponential decay functional form; further work is needed to validate this observation.

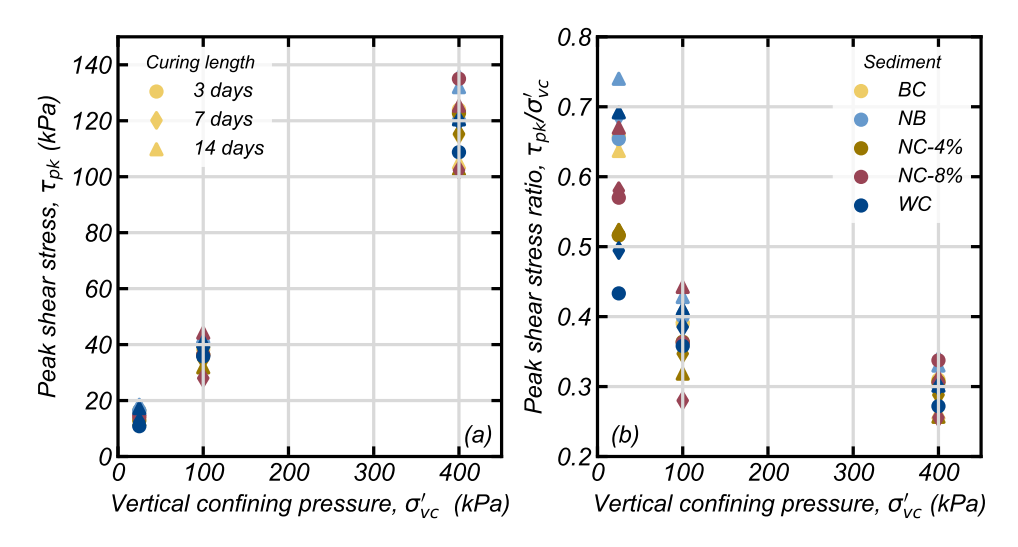


Figure 3:(a) Peak shear stress and (b) peak shear stress ratio versus vertical confining pressure

The four sediments broadly produced similar stress-strain responses across the three σ'_{vc} used. Fig. 4 below presents the stress-strain responses for the different sediments after 3, 7, and 14 days of curing. Generally, all observed stress-strain responses exhibit ductile behavior with τ_{pk} mobilized at an increasing shear strain magnitude as σ'_{vc} increases. At $\sigma'_{vc}=400$ kPa, τ_{pk} is mobilized between approximately 5-10% shear strain, whereas at $\sigma'_{vc}=25$ kPa, τ_{pk} is mobilized at approximately 1-2% shear strain. This difference is likely due to two factors: (1) the increased impact of the cement bonds at lower σ'_{vc} and (2) the potential for cement bond breakage due to consolidation to the larger σ'_{vc} . At higher σ'_{vc} , minimal post-peak strength loss occurs whereas at lower σ'_{vc} post-peak strain hardening is observed. The post-peak strain hardening at low σ'_{vc} is better illustrated in Fig 5 which presents the stress-strain responses expressed as stress ratios. Post-peak hardening generally begins to mobilize at strain levels consistent with τ_{pk} mobilization at larger σ'_{vc} .

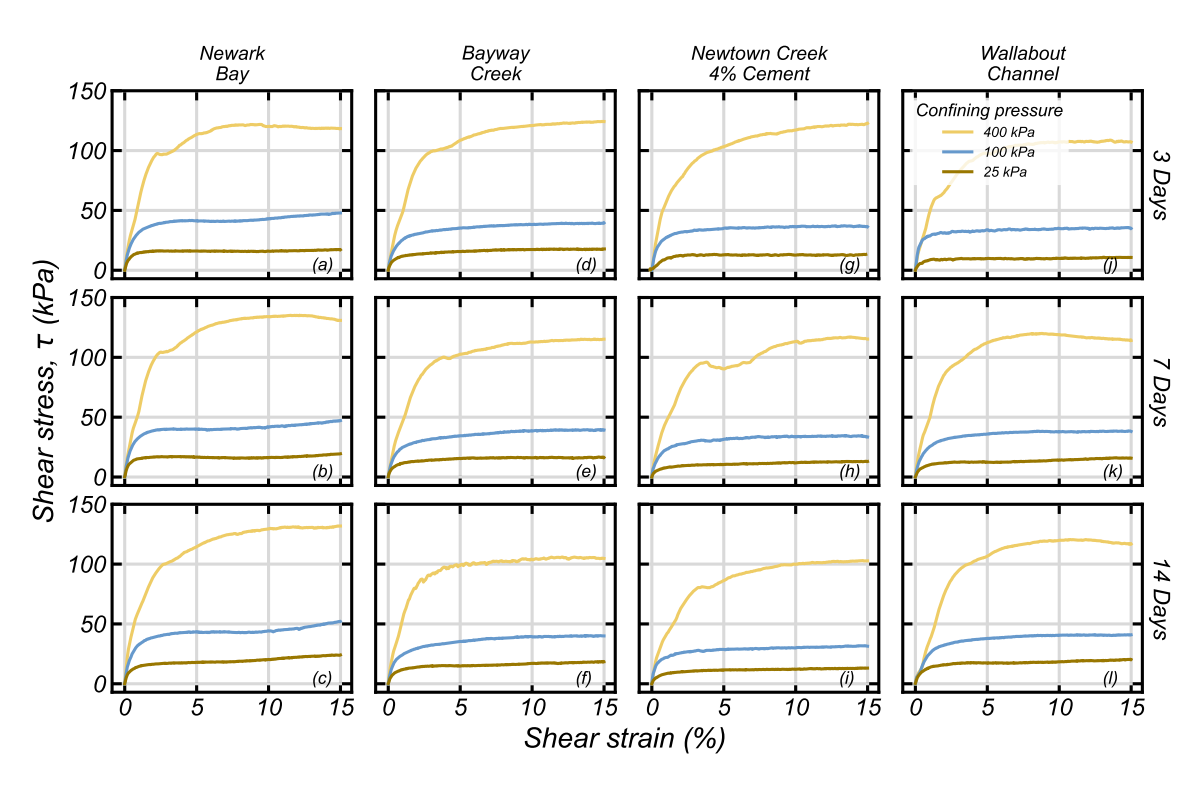


Figure 4: Monotonic stress-strain responses for the sediments stabilized with 4% cement after 3, 7, and 14 days of curing

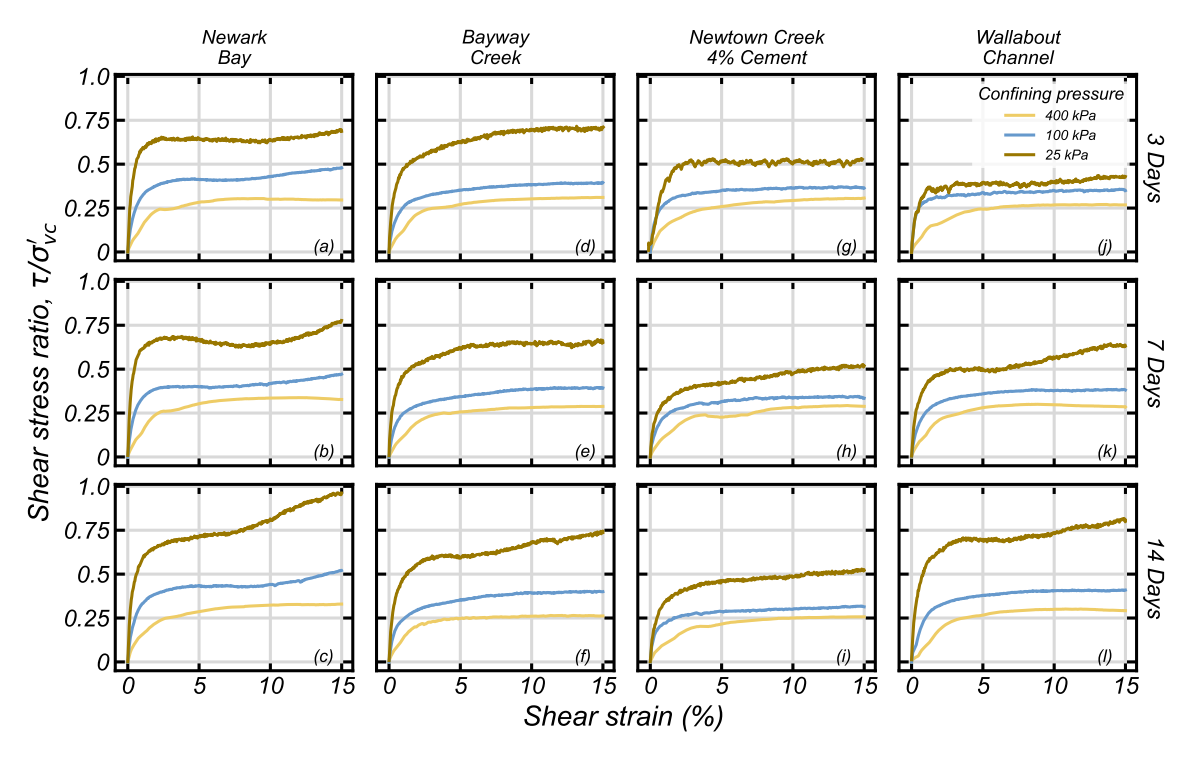


Figure 5: Monotonic stress-strain responses expressed as stress-ratios for the sediments stabilized with 4% cement after 3, 7, and 14 days of curing

At σ'_{vc} = 25 kPa, the strain-hardening coincides with stress paths that are initially

contractive before undergoing a phase transformation and beginning to dilate. Fig. 6 and 7 present the stress-paths for the DSS tests expressed as stresses and stress ratios, respectively. At σ'_{vc} = 400 kPa, all stress paths have contractive tendencies with a decreasing vertical effective stress (σ'_{v}) as τ increases, consistent with a material that is loose of critical state. At σ'_{vc} = 25 kPa, most of the tests (except for NC-4%) exhibit initially contractive behavior followed by dilative behavior, consistent with a material that is dense of critical state. NC-4% does not show a marked phase transformation, however it is unclear if dilation will still occur at shear strain levels beyond what was mobilized in this testing program. At σ'_{vc} = 100 kPa, NB exhibits dilative behavior after all curing durations whereas none of the other three materials present dilative tendencies. It is unclear if this difference is due to material differences which result in significantly different critical state lines, different initial void ratios relative to the critical state line, or if it is a function of the testing approach and dilation will initiate at larger strain levels. Further work is needed to establish the critical state line for these sediments and evaluate whether these materials are loose or dense of critical state and thus whether dilative behavior would still be expected.

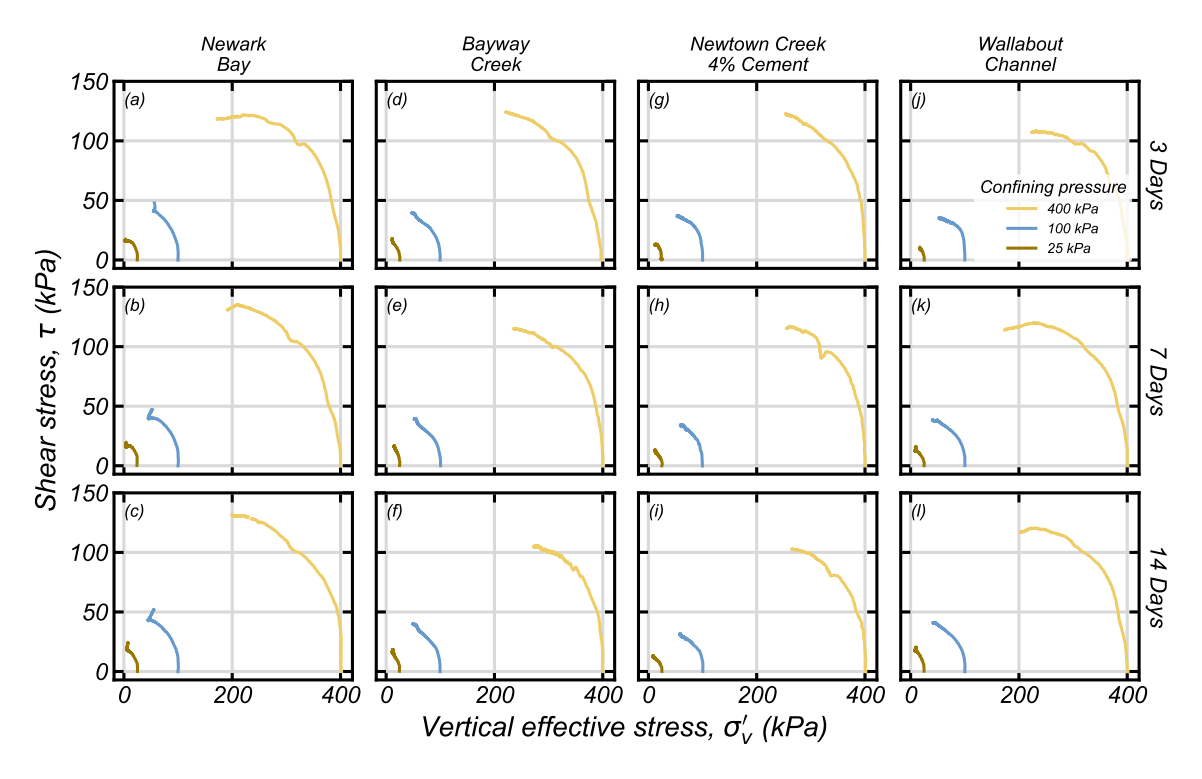


Figure 6: Monotonic stress-paths for the sediments stabilized with 4% cement after 3, 7, and 14 days of curing

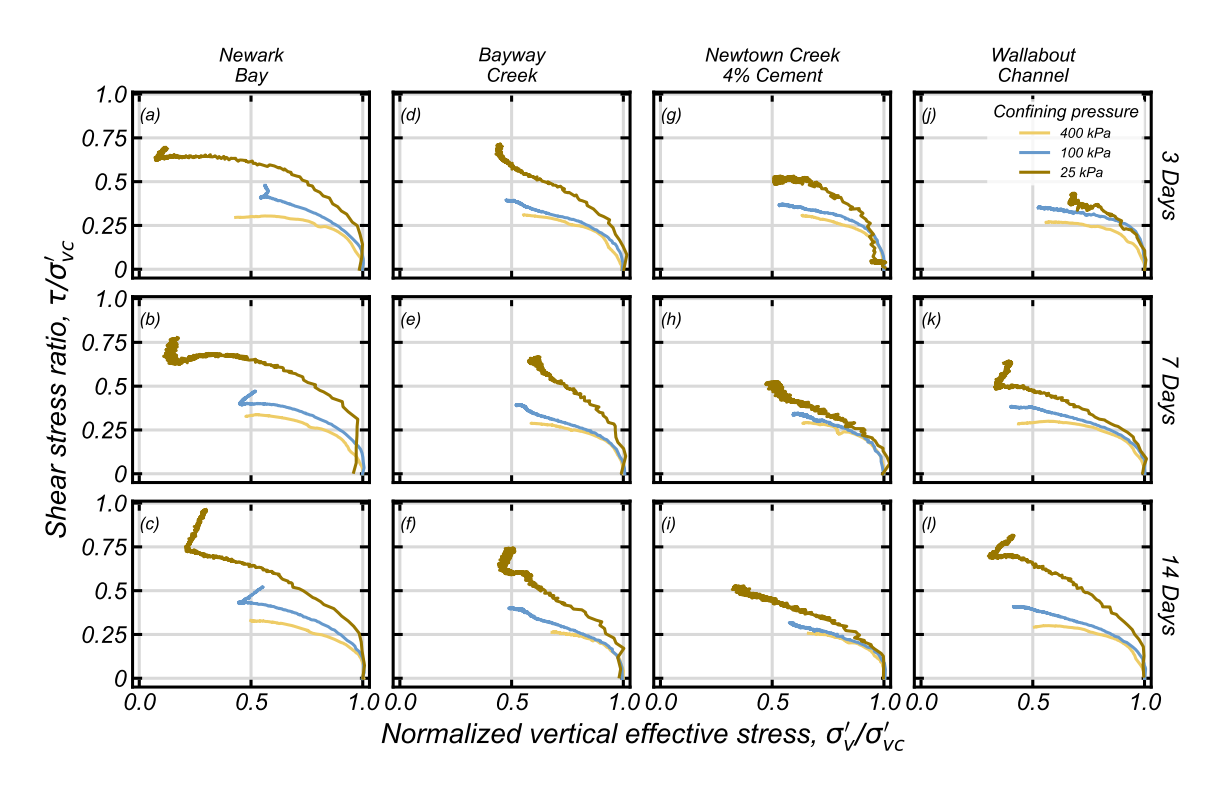


Figure 7: Monotonic stress paths expressed as stress ratios for the sediments stabilized with 4% cement after 3, 7, and 14 days of curing

The impact of the cement content was investigated using the NC sediment. Fig. 8 below presents a comparison of the stress-strain responses and stress paths for the 4% and 8% cement content tests on NC sediment. At σ'_{vc} = 25 kPa, the added cement content produces a noticeable increase in the mobilized τ/σ'_{vc} as well as increased small strain-stiffness, as expected due to the additional bonding producing by the increased cement content. There is no clear relationship between the cement content and the observed response at higher σ'_{vc} . After three days of curing there is negligible difference in the mobilized τ/σ'_{vc} , after 7 days of curing there is negligible difference at σ'_{vc} = 400 kPa while at σ'_{vc} = 100 kPa the 8% response is weaker than the 4% response, and after 14 days of curing the 8% cement response is stronger at both σ'_{vc} = 100 kPa and 400 kPa. Additional work is needed to robustly investigate the differences between the 4% and 8% cement content under direct simple shear loading.

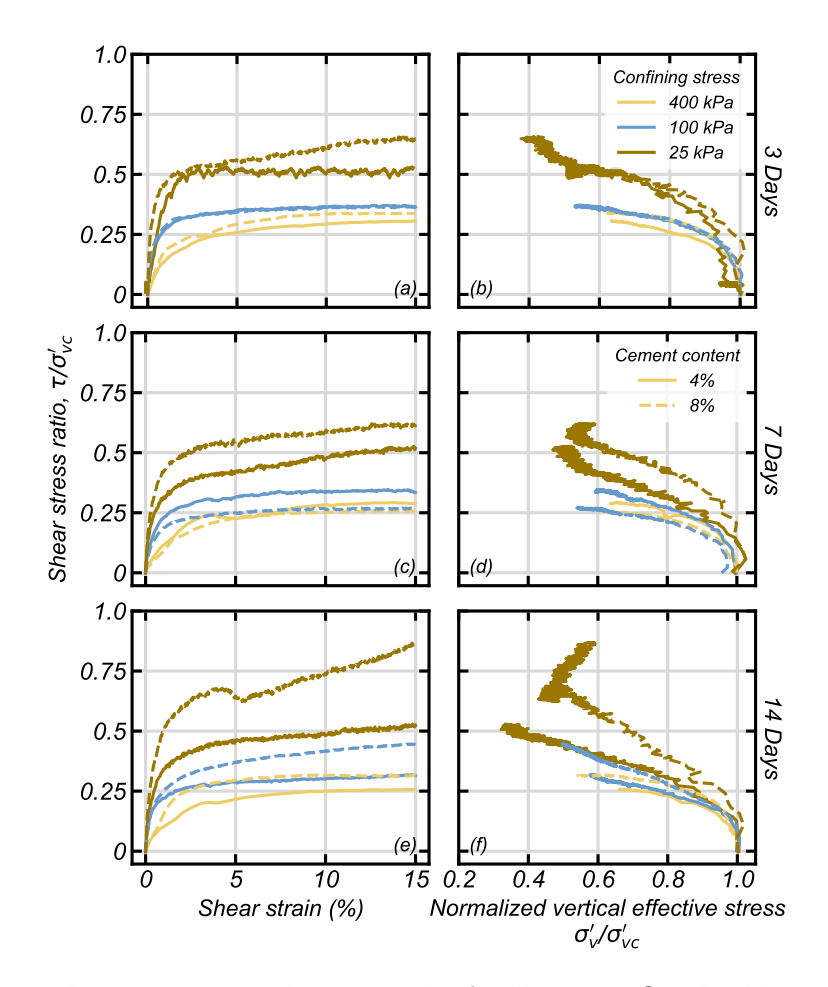


Figure 8: Stress-strain responses and stress paths for Newtown Creek with 4% and 8% added cement after 3, 7, and 14 days of curing

Three additional DSS tests were performed at σ'_{vc} = 100 kPa on samples of NB sediment after curing for 28 days, 3 months, and 6 months respectively to investigate how long-term curing impacts the response of the sediment. Figure 9 below presents the stress-strain response and stress-path of the tests. Increasing the curing time generally increases the τ_{pk} mobilized at 15% shear strain, except for the sediment after six months curing which has a lower τ_{pk} . This may be due to changes in the bonding between the water and the cement within the soil-sediment-cement matrix or is an outlier due to inherent sediment variability. Further work is needed to investigate this observation. As the curing duration increases, the sediments generally undergo phase transformation and begin to dilate at lower magnitudes of shear strain indicating the cementation is continuing to impact the stress strain response. This tracks with stress paths that continue to remain stiffer as curing duration increases. The stress-paths during dilation have a similar slope indicating that the material is undergoing a similar frictional response but is potentially offset by differences in the cementation.

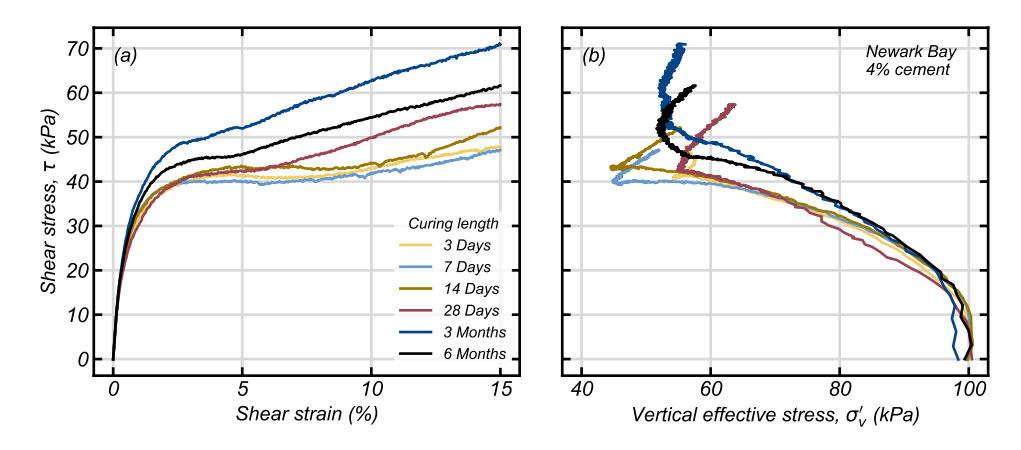


Figure 9: Impact of long-term curing on stress-strain response of Newark Bay sediment tested at a σ'_{vc} = 100 kPa

The results of the DSS tests can be used to interpret the Mohr-Coulomb failure criteria represented by a friction angle and a cohesion intercept. Table 3 below presents the interpreted friction angle and cohesions for the sediment after each curing length. At σ'_{VC} = 25 kPa, where some tests undergo strain-hardening, MC properties were interpreted based on the τ_{pk} prior to subsequent strain-hardening. Generally, the interpreted cohesion increases with increasing curing duration, consistent with the ongoing curing of the cement in the soil matrix. The increase in cohesion ranges from approximately 11% for the NC with 4% cement to ~120% for the WC sediment. The tPAH content of the sediment appears to impact how the interpreted friction angle changes with curing duration. At low tPAH values (NB and WC sediments), the friction angle increases with an increasing curing duration. However, at high tPAH values, the friction angle either decreases (BC and NC-4%) or has no clear pattern (NC-8%) as the curing duration increases. This difference might be attributed to the higher tPAH concentrations inhibiting the ability of the added cement to bind with the water in the matrix and reduces the impact of the cement on the stabilization. Further work is needed to systematically evaluate this across a range of DSS loading conditions and sediment/binder types.

Table 3: Interpreted and optimized friction angle and cohesion

		Inter	preted	Optii	mized
Sediment	Curing Length (days)	Friction Angle (°)	Cohesion (kPa)	Friction Angle (°)	Cohesion (kPa)
	3	23.5	13.3	24	10.8
Newark Bay	7	30.1	13.5	24	11
	14	30.1	16.1	24	12
\/\allahaut	3	23.7	7.5	22	5
Wallabout	7	25.2	13.5	23	7.5
Channel	14	25.1	16.5	22.5	12
	3	26.9	12.2	24	11.5
Bayway Creek	7	23.7	12.5	21.5	10.5
	14	18.3	16.1	19	14
Newtown Creek 4% Cement	3	24.1	9.6	23	7
	7	22.7	8.4	21	7.5
	14	19.2	10.7	18	7.5
Newtown Creek	3	27.9	7.5	24	7.5

8% Cement	7	21.3	8.3	18	7.5
	14	27.5	13.8	23	11

3.2 UCS

The UCS strength is a function of the individual sediment characteristics (density and moisture content) and curing duration. Fig. 10 below presents the UCS versus (a) density, (b) moisture content, and (c) curing length while Table 4 summarizes the results. Generally, the densities are approximately 1.4 g/cm³ (BC and NB) or approximately 1.25 g/cm³ (NC and WC) and remains constant across the different curing durations. The density range is consistent with the observed initial moisture contents, specific gravities, and organic contents. The sediments with higher average densities typically align with lower moisture contents and sediments with lower average densities typically align with higher moisture contents at testing. Higher densities and lower moisture contents generally correspond with higher UCS strengths at all curing durations (Fig. 10 a,b). The UCS increases with increasing curing length for all sediments except for NC with 4% portland cement where minimal strength gain is observed between 3 and 7 days of curing (Fig. 10c). Overall, the results of the UCS tests are consistent with observations of strength gain in the DSS tests at lower confining pressures with additional curing time.

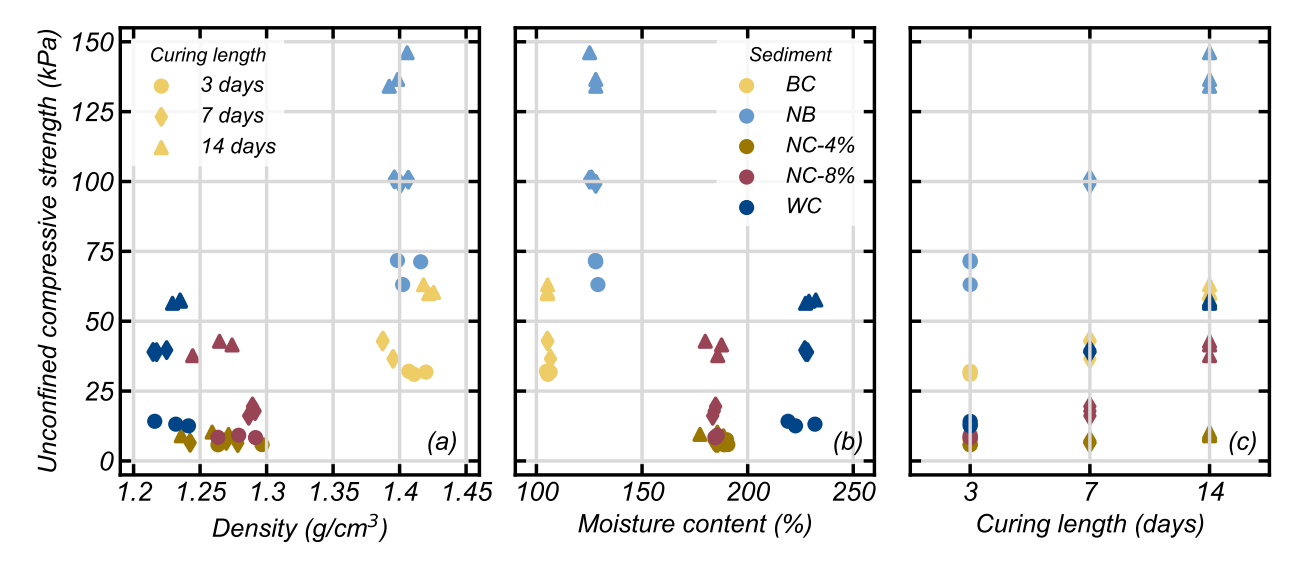


Figure 10: Unconfined compressive strength versus (a) density, (b) moisture content, and (c) curing length

Table 4: Results of UCS testing program

Sediment	Curing	Density (g/cm³)		Moisture content (%)		UCS (kPa)	
Sediment	length (days)	μ	σ	μ	σ	μ	σ
	3	1.41	0.005	105.5	0.7	31.6	0.5
Bayway	7	1.39	0.004	105.7	0.7	40.8	3
	14	1.42	0.003	105.2	0.0	61.1	1.4
	3	1.41	0.007	128.4	0.5	68.7	4
Newark	7	1.4	0.004	126.5	1.2	100.2	0.7
Bay	14	1.4	0.006	127.1	1.4	138.9	5.2
N	3	1.27	0.15	189.8	0.7	6.4	0.8
Newtown Creek 4%	7	1.26	0.015	185.0	0.7	6.7	0.3
CIEER 4 /6	14	1.25	0.015	183.9	4.7	9.6	0.5
N.I.	3	1.28	0.012	185.0	0.5	8.7	0.4
Newtown	7	1.29	0.002	184.1	0.6	17.8	1.4
Creek 8%	14	1.26	0.012	184.5	3.3	40.7	2.2
	3	1.23	0.01	224.5	5.4	13.3	0.7
Wallabout Channel	7	1.22	0.004	227.7	0.5	39.2	0.3
Channel	14	1.23	0.003	229.5	2.0	57.1	0.5

4. NUMERICAL MODELING

The numerical modeling aimed to investigate the ability to numerically simulate the deformation response of the stabilized sediment using the experimental DSS tests as a baseline. The Mohr-Coulomb constitutive model was used as the primary constitutive model due to its common use in practice and relatively simple input parameters: density, shear modulus, bulk modulus, friction angle, and cohesion. The Mohr-Coulomb (MC) constitutive model separates the elastic and plastic portion of the response and as such is not expected to capture higher level behaviors such as the response under cyclic loading or the stress path, however it generally is able to reasonably capture the monotonic stress-strain response of soils. Additionally, the baseline MC model utilized in this analysis is unable to capture the secondary strain-hardening, so the focus is on predicting the τ_{pk} mobilized prior to secondary hardening whenever the experimental results predicted strain-hardening. This is a conservative approach and likely mimics how strain-hardening would be accounted for in practice.

MC calibrations were developed for all combinations of sediments and cement contents (15 total combinations). The MC calibrations were developed in two stages: (1) utilizing the interpreted friction angle and cohesion from the DSS tests and (2) adjusting the friction angle and cohesion to best match the stress-strain responses at the different confining pressures. All calibrations used a shear modulus of 5065 kPa, which was found to reasonably approximate the initial stiffness of the stress-strain response and assumed a Poisson's ratio of 0.3 to calculate the bulk modulus. The shear modulus was selected to match the stress-strain response and does not represent a maximum shear modulus (G_{max}) that is necessary for other analysis types. Densities were calculated based on the specific gravity and an assumed initial void ratio. As the simulations were single element, constant volume (a proxy for undrained) with a prescribed confining pressure, the density does not significantly impact the results of the simulations compared to the other parameters or modeling choices. A small subset of sediment and curing length combinations

were simulated with the PM4Silt constitutive model to investigate the ability of more advanced models to capture the deformation response as well as the stress path of the material; something that is not possible with the MC model.

4.1 MOHR-COULOMB WITH EXPERIMENTALLY INTERPRETED PROPERTIES

Using the friction angle and cohesion interpreted from the Mohr circles of the experimental tests for the calibrations generally results in τ_{pk}/σ'_{vc} in the model which are larger than those that are observed in the experimental tests. Fig. 11a presents the measured τ_{pk}/σ'_{vc} versus the modeled τ_{pk}/σ'_{vc} using the interpreted properties relative to a 1:1 line. The data points generally follow a linear trend however they are offset above the line 1:1 line indicating a systematic overprediction of the τ_{pk}/σ'_{vc} . The interpreted parameters capture the experimental response with different levels of success depending on the sediments and curing time.

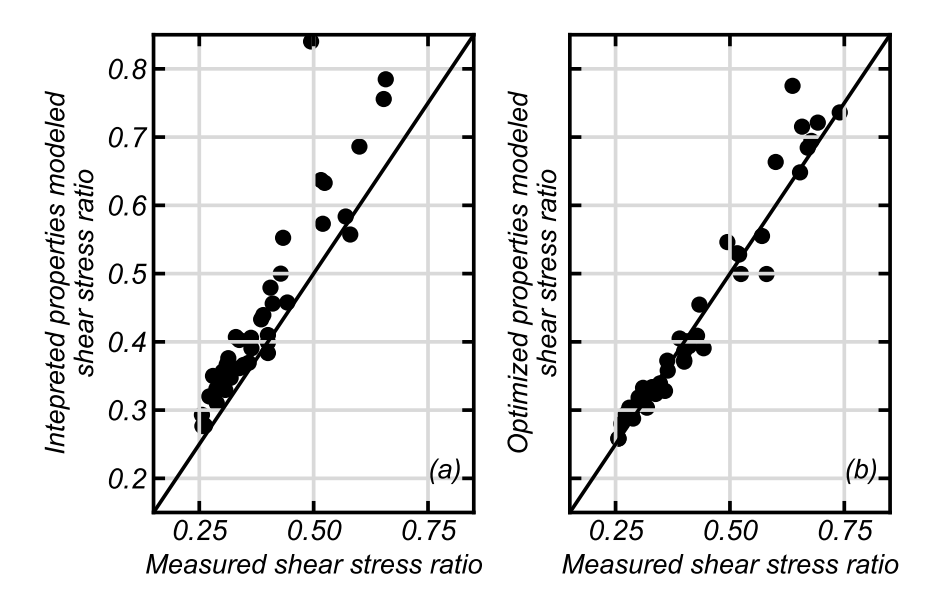


Figure 11: Measured peak shear stress ratio versus the maximum shear stress ratio modeled using (a) interpreted and (b) optimized friction angle and cohesion

Fig. 12 below presents the stress-strain response and stress path for a selected subset of calibrations which illustrate the range of modeled responses relative to the experimental results. Fig. 12 a/b shows the calibrations for NB after 3 days of curing which represent the experimental responses reasonably well. Fig. 12 c/d presents the results for NB after 7 days of curing where the interpreted properties significantly overestimated the peak strengths at all consolidation levels. Fig. 12 e/f presents the results for WC after 14 days of curing which also shows a systematic over prediction. Generally, the examples shown in Fig. 12 represent the trends across all 15 calibrations. While different levels of success were observed in capturing τ_{pk} , at all σ'_{vc} the calibrations align well with initial stiffness of the stress-strain response. However, at lower σ'_{vc} the model underpredicts the stiffness degradation which results in τ_{pk} being mobilized at smaller shear strain levels than the experimental results indicate. This is expected due to the formulation of the MC model separating the elastic and plastic regimes and is consistent with the inability of the MC model to capture the decrease in σ'_{v} shown in the experimental stress path (Fig. 12 b,d,e). These observations suggest that moderate adjustments to the Mohr-Coulomb parameters might result in modeled responses that better align with the experimental results; however, the parameter changes will not result in better approximation of the stress paths or stiffness degradation.

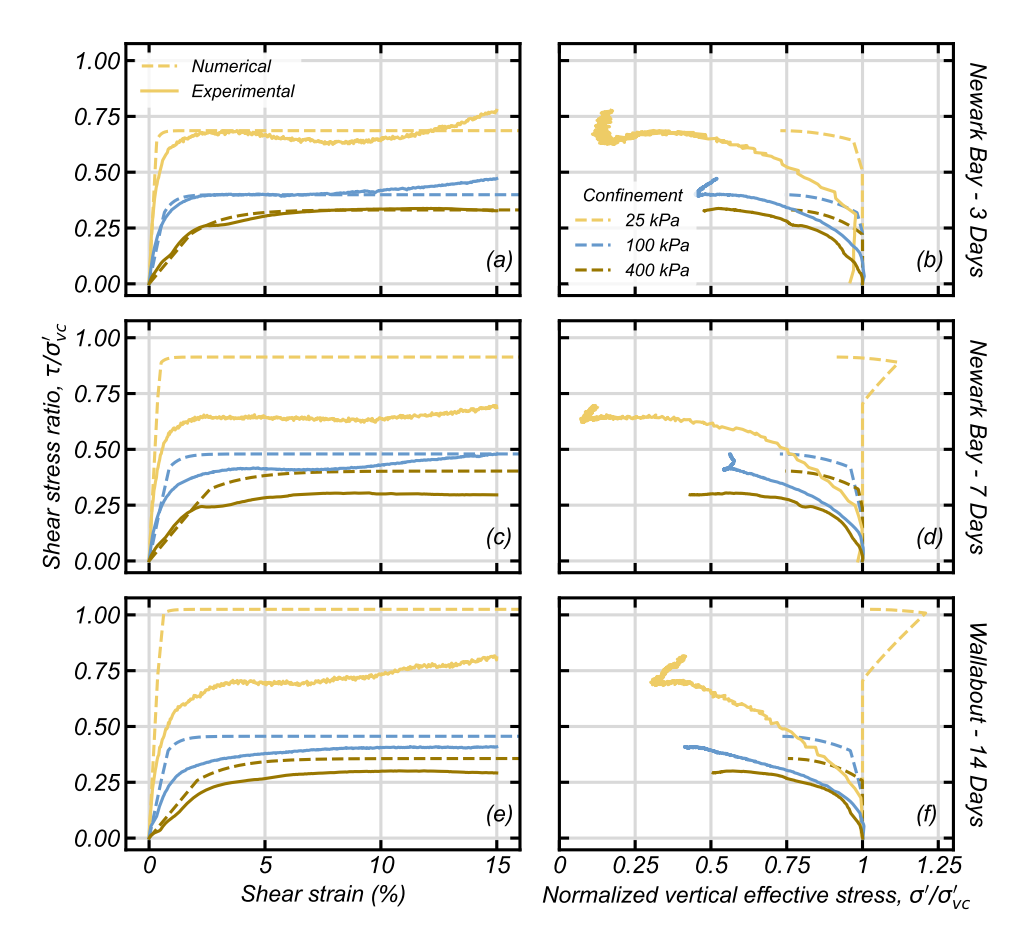


Figure 12: Comparison between the measured and predicted response using the interpreted properties expressed as (a,c,e) stress strain responses and (b,d,e) stress paths for Newark Bay after 3 days curing (a,b), Newark Bay after 7 days curing (c,d), and Wallabout Channel after 14 days of curing (e,f)

4.2 MOHR-COULOMB WITH ADJUSTED PROPERTIES

The calibrations were redeveloped to better capture the experimental results using the interpreted properties as a baseline. The goal of the adjustments was to develop a calibration that approximated the stress-strain responses across the different σ'_{vc} as well as possible while making only as minor of changes as necessary to the interpreted properties as possible. The friction angle and cohesion were iteratively adjusted as follows:

- 1. The friction angle was adjusted to provide a reasonable approximation of the stress-strain response for σ'_{vc} = 400 kPa as that result is relatively independent of the cohesion due to the high σ'_{vc} .
- 2. Cohesion was adjusted to provide a reasonable approximation of the stress-strain response for σ'_{vc} = 25 kPa as the behavior at that stress level is primarily dependent on the cohesion.
- 3. The response was evaluated for reasonableness against the σ'_{vc} = 100 kPa which is impacted by both the friction angle and the cohesion.
- 4. Steps 1-3 were iterated as needed until the fit with all three stress-strain responses was as reasonable as possible.

Overall, the final adjusted properties resulted in decreased friction angles and cohesions

compared with their interpreted values. Fig. 13 below presents the interpreted versus adjusted friction angles (Fig. 13a) and cohesions (Fig. 13b). The cohesion was typically reduced by approximately 2 or 3 kPa for all calibrations. The friction angle had a larger reduction at higher interpreted friction angles and the largest adjusted friction angle was ~24° compared with the largest interpreted friction angle being ~30°. The adjustments to the soil properties results in modeled τ_{pk}/σ'_{vc} that are aligned well with the measured τ_{pk}/σ'_{vc} as shown by the data being approximately normally distributed about the 1:1 line in Fig. 11b.

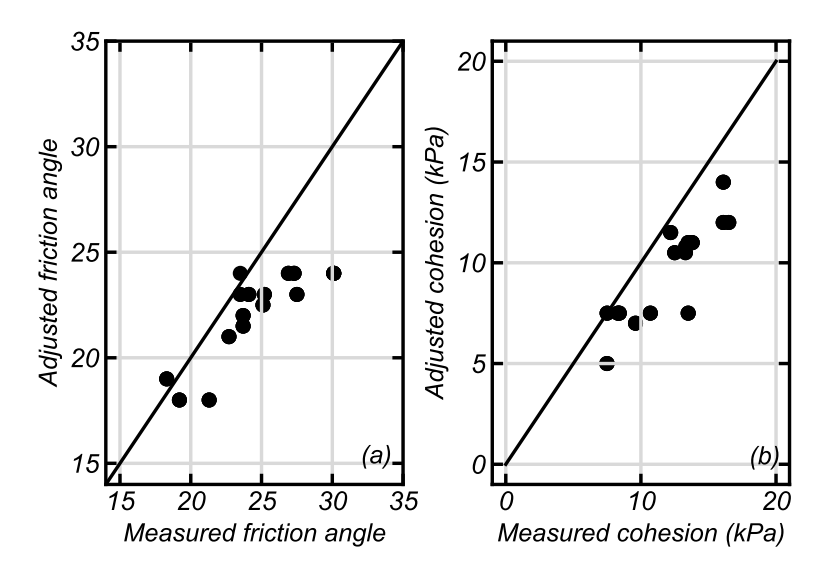


Figure 13: Experimentally interpreted versus measured (a) friction angle and (b) cohesion

The optimization of the friction angle and the cohesion resulted in predicted stress-strain responses which much more reasonably approximated the experimental results. Fig. 14 below presents the stress-strain responses and stress paths for the three calibrations highlighted in Fig. 12. As shown, the predicted stress-strain responses much more accurately capture the experimental results. However, as discussed prior, the stress path is still predicted to remain stiffer due to the lack of accumulated plastic strain prior to yielding and the associated lack of pore pressure generated.

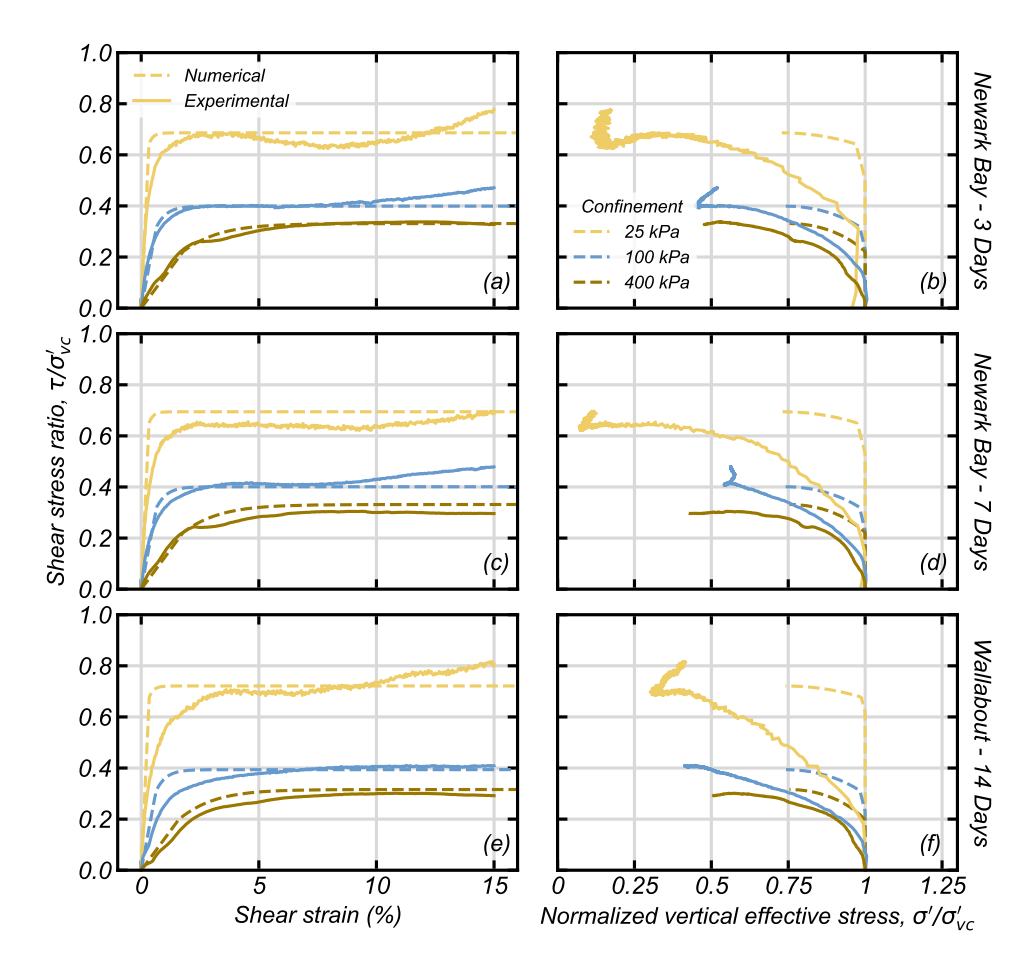


Figure 14: Comparison between the measured and predicted response using the adjusted properties expressed as (a,c,e) stress strain responses and (b,d,e) stress paths for Newark Bay after 3 days curing (a,b), Newark Bay after 7 days curing (c,d), and Wallabout Channel after 14 days of curing (e,f)

4.3 PM4SILT MODELING

To attempt to address limitations of the MC model, particularly the inability to capture the stress-path of the material and the related inability to predict the pore pressure generation, the PM4Silt constitutive model was utilized. PM4Silt calibrations were developed for the three combinations shown in Fig. 12 and 14. The goal was to investigate whether a more advanced constitutive model can capture a broader range of material responses and in-turn provide a pathway to investigate more robust structures and loading conditions such as embankments during earthquake or storm loading.

PM4Silt is a critical state compatible, stress-ratio controlled, bounding surface plasticity model developed for use simulating plastic silts and clays. The model has three required input parameters: (1) the shear modulus coefficient (G_o), (2) the contraction rate parameter (h_{po}), (3) the critical state undrained strength ($s_{u,cs}$) or undrained strength ratio ($s_{u,cs}/\sigma'_{vc}$). There are approximately 20 secondary parameters that are assigned default values or can be modified based on site-specific data. This work will leave the secondary parameters as their default values due to the limited available information and focus on the three primary parameters. All calibrations utilized a h_{po} of 20.

Calibrations utilized the $s_{u,cs}$ parameter instead of the $s_{u,cs}/\sigma'_{vc}$ parameter as the undrained shear strength ratio of the sediment varied with σ'_{vc} due to the changing influence of the cementation. Initial calibrations utilized the same G_o parameter for all σ'_{vc} ; however, this was shown to only accurately predict the stress-strain response at a single σ'_{vc} while severely over or underestimating the stiffness at the other σ'_{vc} responses. This is likely due to breaking of cementation bonds at higher σ'_{vc} reducing the stiffness at smaller strain levels. This is more impactful in models which immediately have plastic behavior such as PM4Silt compared with the MC model that is initially elastic. To address this, the calibrations utilized a stress-dependent G_o , representing a decreasing shear modulus as σ'_{vc} increases. Ultimately the calibrations varied two parameters ($s_{u,cs}$ and G_o) with selected parameters shown in Table 5 below. The G_o for Newark Bay did not change between 3 and 7 days of curing indicating the small strain stiffness may not be impacted by the additional curing.

Table 5: Parameters for PM4Silt calibrations

Sediment	Parameter*	$\sigma'_{vc} = 25 \text{ kPa}$	$\sigma'_{vc} = 100 \text{ kPa}$	$\sigma'_{vc} = 400 \text{ kPa}$
Nowark Pay 2 Days	G_{\circ}	500	150	50
Newark Bay 3 Days	Su	16500	42000	120100
Newark Bay 7 Days	G。	500	150	50
	Su	16950	40560	135000
Wallabout Channel 14 Days	G。	400	100	35
	S_{u}	17300	41050	120500

^{*}All other parameters retain their default values except for the contraction rate parameter ($h_{po} = 20$).

The PM4Silt calibrations are shown to capture the stress-strain response well and better match the stress paths of the material. Fig. 15 below presents the stress-strain responses and stress paths for the experimental data compared to the PM4Silt simulations. The stress-strain responses for all three calibrations are able to better match both the mobilized peak strength as well as the strain at mobilization and degradation of shear stiffness for all σ'_{vc} (Fig. 15 a,c,e). Additionally, the stress paths better match the experimental responses compared with the MC model. The stress-paths initially begin to shed σ'_{v} as pore pressures are generated, consistent with the experimental results. For all σ'_{vc} , less pore pressure is generated in the PM4Silt simulations compared to the experimental results, this is likely because PM4Silt does directly incorporate cementation but rather is proxying the effect of cementation by changing the su. This also may contribute to why the PM4Silt calibration at σ'_{vc} = 25 kPa has more significant dilation compared to the experimental result. The PM4Silt calibration assumes a denser material to mobilize the high strength rather than assuming a loose (contractive) material with cementation contributing to the strength. Regardless, both the stress-strain responses and stress paths are captured reasonably well by PM4Silt suggesting that the model may be appropriate for use given certain safeguards and checks during analyses.

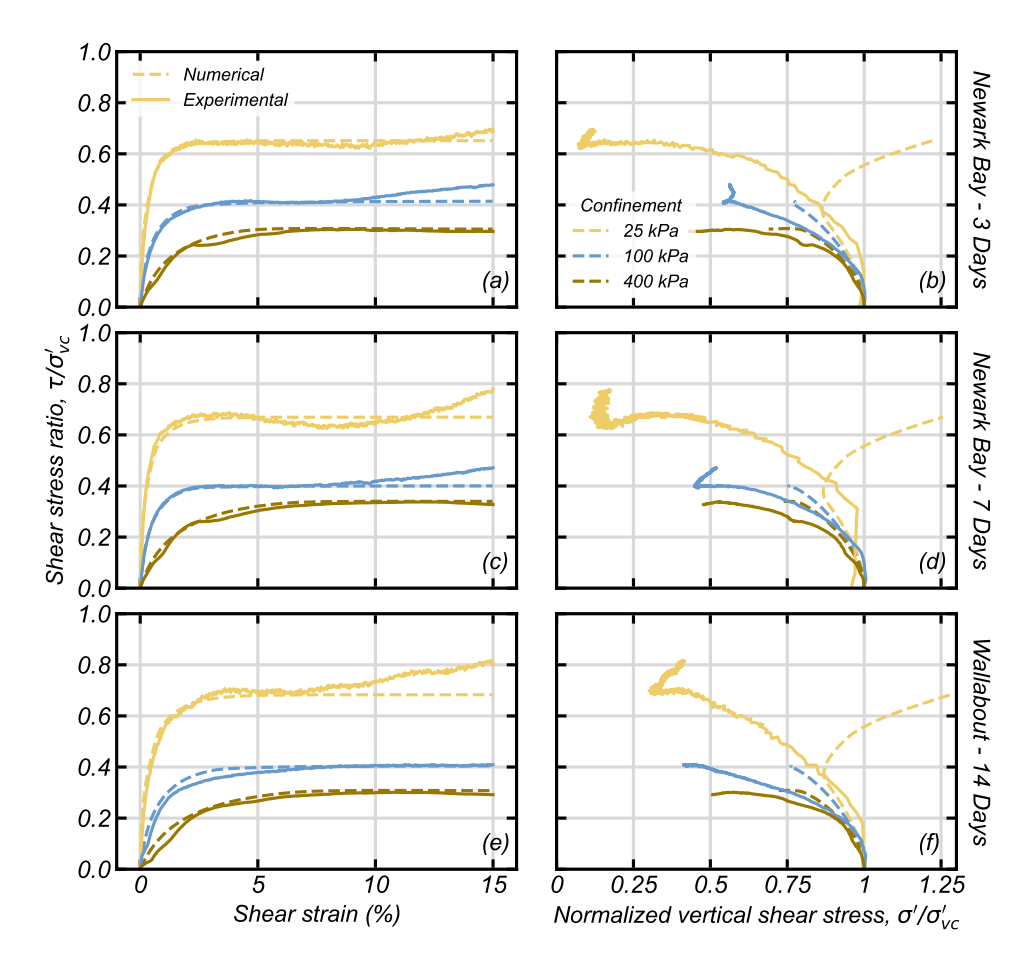


Figure 15: Comparison between the measured and predicted response using PM4Silt expressed as (a,c,e) stress strain responses and (b,d,e) stress paths for Newark Bay after 3 days curing (a,b), Newark Bay after 7 days curing (c,d), and Wallabout Chanel after 14 days of curing

5. CONCLUSIONS

This project investigated the deformation tendencies of stabilized sediments from the New York and New Jersey Harbor under direct simple shear loading conditions. Sediments were tested after different curing durations and with different vertical confining pressures. The experimental results indicated a less brittle response than expected and that generally the material behaved like other soft soils. The experimental test results were then used as baseline data for calibrating different constitutive models. The Mohr-Coulomb model was shown to reasonably approximate the stress-strain response of the material but was unable to capture the pore pressure generation and stress path. The more complex PM4Silt model was shown to be capable of capturing the stress-strain response, pore pressure generation, and stress path of the sediment reasonably well.

This research program illustrated that the deformation tendencies of stabilized sediment may not be as brittle as seen in UCS tests when they are loaded under confinement. This less brittle behavior may likely be encountered in practice as all sediment except for surficial sediment is loaded under confinement in the field. These observations may open opportunities for using stabilized sediment in projects with more stringent design requirements. Additionally, the ability

of both the Mohr-Coulomb and the PM4Silt model to accurately capture the deformation tendencies further extends the potential of using sediment in more complex projects that require numerical modeling in the design process. While these initial insights look promising, this was only a preliminary investigation. Further work is needed to translate these results into practice including accounting for curing under confinement, the construction timeline, different sediment types, different binder types and proportions, upscaling modeling results to the system scale, and evaluating the behavior under more complex loading conditions such as cyclic loading.

6. REFERENCES

- Boulanger, R. W., and Ziotopoulou, K. (2019). "A constitutive model for clays and plastic silts in plane-strain earthquake engineering applications." Soil Dynamics and Earthquake Engineering, 127(2019): 105832, 10.1016/j.soildyn.2019.105832.
- Chew, S. H., A. H. M. Kamruzzaman, and F. H. Lee. 2004. "Physicochemical and Engineering Behavior of Cement Treated Clays." *Journal of Geotechnical and Geoenvironmental Engineering* 130, no. 7: 696-706. https://doi.org/10.1061/(ASCE)1090-0241(2004)130:7(696).
- Chompoorat, T., T. Maikhun, and S. Likitlersuang. 2019. "Cement Improved Lake Bed Sedimentary Soil for Road Construction." *Proceedings of the Institution of Civil Engineers Ground Improvement* 172: 1-37. https://doi.org/10.1680/jgrim.18.00076.
- Dermatas, D., P. Dutko, J. Balorda-Barone, and D. H. Moon. 2003. "Geotechnical Properties of Cement Treated Dredged Sediment to be Used as Transportation Fill." *Dredging, Key Technologies for Global Prosperity*: 1-14. https://doi.org/10.1061/40680(2003)139.
- Grubb, Dennis G., Nicholas E. Malasavage, Charles J. Smith, and Maria Chrysochoou. 2010. "Stabilized Dredged Material. II: Geomechanical Behavior." *Journal of Geotechnical and Geoenvironmental Engineering* 136, no. 8: 1011-1024. https://doi.org/10.1061/(ASCE)GT.1943-5606.0000290.
- Horpibulsuk, S., R. Rachan, A. Chinkulkijniwat, Y. Raksachon, and A. Suddeepong. 2010. "Analysis of Strength Development in Cement-Stabilized Silty Clay from Microstructural Considerations." *Construction and Building Materials* 24, no. 10: 2011–2021. https://doi.org/10.1016/j.conbuildmat.2010.03.011.
- Horpibulsuk, S., R. Rachan, and A. Suddeepong. 2011. "Assessment of Strength Development in Blended Cement Admixed Bangkok Clay." *Construction and Building Materials* 25, no. 4: 1521–1531.
- Horpibulsuk, Suksun, Norihiro Miura, and D. T. Bergado. 2004. "Undrained Shear Behavior of Cement Admixed Clay at High Water Content." *Journal of Geotechnical and Geoenvironmental Engineering* 130, no. 10: 1096-1103. https://doi.org/10.1061/(ASCE)1090-0241(2004)130:10(1096).
- Lirer, S., B. Liguori, I. Capasso, A. Flora, and D. Caputo. 2017. "Mechanical and Chemical Properties of Composite Materials Made of Dredged Sediments in a Fly-Ash Based Geopolymer." *Journal of Environmental Management* 191: 1-7.
- Itasca (2019). FLAC Fast Lagrangian Analysis of Continua, Version 8.1, Itasca Consulting Group, Inc., Minneapolis, Minnesota.

- Liu, C., and Ryan D. S. 2013. "Effects of Curing Conditions on Unconfined Compressive Strength of Cement- and Cement-Fiber-Improved Soft Soils." *Journal of Materials in Civil Engineering* 25: 1134-1141. https://doi.org/10.1061/(ASCE)MT.1943-5533.0000575.
- Maher, Ali, W. Scott Douglas, Farhad Jafari, and Joel Pecchioli. 2013. "The Processing and Beneficial Use of Fine-Grained Dredged Material: A Manual for Engineers." Center for Advanced Infrastructure and Transportation, Rutgers University. https://cait.rutgers.edu/wp-content/uploads/2018/05/193-ru2763_1.pdf.
- Pakbaz, M. S., and R. Alipour. 2012. "Influence of Cement Addition on the Geotechnical Properties of an Iranian Clay." *Applied Clay Science* 67-68: 1–4. https://doi.org/10.1016/j.clay.2012.07.006.
- Ranaivomanana, H., A. Razakamanantsoa, and O. Amiri. 2018. "Effects of Cement Treatment on Microstructural, Hydraulic, and Mechanical Properties of Compacted Soils: Characterization and Modeling." *International Journal of Geomechanics* 18, no. 9. https://doi.org/10.1061/(ASCE)GM.1943-5622.0001248.
- Sariosseiri, F., and B. Muhunthan. 2009. "Effect of Cement Treatment on Geotechnical Properties of Some Washington State Soils." *Engineering Geology* 104, no. 1-2: 119-125. https://doi.org/10.1016/j.enggeo.2008.09.003.
- Snellings, R., Ö. Cizer, L. Horckmans, P. T. Durdziński, P. Dierckx, P. Nielsen, K. Van Balen, and L. Vandewalle. 2016. "Properties and Pozzolanic Reactivity of Flash Calcined Dredging Sediments." *Applied Clay Science* 129: 35-39. https://doi.org/10.1016/j.clay.2016.04.019.
- Suzuki, M., T. Fujimoto, and T. Taguchi. 2014. "Peak and Residual Strength Characteristics of Cement-Treated Soil Cured Under Different Consolidation Conditions." *Soils and Foundations* 54, no. 4: 687-698. https://doi.org/10.1016/j.sandf.2014.06.023.
- Talebi, M., Oathes, T., Miskewitz, R., Arnold, K., Pharande, E., 2025." Monotonic Behavior of Improved Soft Sediment under Direct Simple Shear Loading" Geo-Frontiers 2025 (ASCE).
- Voottipruex, P., and P. Jamsawang. 2014. "Characteristics of Expansive Soils Improved with Cement and Fly Ash in Northern Thailand." *Geomechanics and Engineering* 6: 437–453.